Experimentally Based Estimates of Relations between X-Band Radar Signal Attenuation Characteristics and Differential Phase in Rain

SERGEY Y. MATROSOV

Cooperative Institute for Research in Environmental Sciences, University of Colorado Boulder, and NOAA/Earth System Research Laboratory, Boulder, Colorado

PATRICK C. KENNEDY

Department of Atmospheric Science, Colorado State University, Fort Collins, Colorado

ROBERT CIFELLI

NOAA/Earth System Research Laboratory, Boulder, Colorado

(Manuscript received 22 October 2013, in final form 13 May 2014)

ABSTRACT

Correcting observed polarimetric radar variables for attenuation and differential attenuation effects in rain is important for meteorological applications involving measurements at attenuating frequencies such as those at X band. The results of estimating the coefficients in the correction-scheme relations from dual-wavelength polarimetric radar measurements of rainfall involving attenuating and nonattenuating frequencies are described. Such coefficients found directly from measurements are essentially free from different assumptions about drop shapes, drop size distributions, and/or relations between different radar variables that are typically used in many attenuation and differential attenuation correction schemes. Experimentally based estimates derived using dual-wavelength radar measurements conducted during a project in northern Colorado indicate values of the coefficients in the attenuation–differential phase quasi-linear relations at X band in the approximate range of 0.20–0.31 dB deg^{-1}. The corresponding coefficients in the differential attenuation–differential phase relations are in the range of 0.052–0.065 dB deg^{-1}.

1. Introduction and objectives

The active use of polarimetric meteorological X-band (wavelength $\lambda \approx 3$ cm) radars for quantitative precipitation estimation (QPE) started about 15 years ago (e.g., Matrosov et al. 2002; Anagnostou et al. 2004) and has been on the increase ever since. Particular interest in measurements at this frequency band is dictated by a relative compactness and low cost of X-band radar systems compared to traditional meteorological radar frequencies at S ($\lambda \approx 10$–11 cm) and C bands ($\lambda \approx 5$ cm), and also by applicability of X-band specific differential phase shift–based rainfall retrievals for lower rain rates than can be done at longer radar wavelengths (e.g., Matrosov et al. 2006). Attenuation of X-band radar signals in rain, however, is significant; thus, special techniques need to be applied to correct observed reflectivity factor Z_{eh} on horizontal polarization (hereafter *reflectivity*) and differential reflectivity Z_{DR} (e.g., Gorgucci and Chandrasekar 2005).

Attenuation correction schemes usually use either a simple differential phase approach (e.g., Matrosov et al. 2002) or a range-profiling approach (e.g., Testud et al. 2000) and its different modifications (e.g., Bringi et al. 2001; Ryzhkov et al. 2014). These approaches rely on the relation between horizontal polarization specific attenuation A_h and specific differential phase shift between horizontally and vertically polarized radar returns K_{DP}:

$$A_h = \alpha K_{\mathrm{DP}}^{\beta}. \tag{1}$$

Theoretical modeling (e.g., Bringi and Chandrasekar 2001; Matrosov et al. 2002) indicates that at X band

Corresponding author address: Sergey Y. Matrosov, R/PSD2, NOAA/Earth System Research Laboratory, 325 Broadway St., Boulder, CO 80305.
E-mail: sergey.matrosov@noaa.gov

DOI: 10.1175/JTECH-D-13-00231.1

© 2014 American Meteorological Society

$\beta \approx 1$. Specific differential attenuation (A_{DP}) correction to Z_{DR} measurements assumes the relation

$$A_{DP} = \gamma K_{DP}^{\zeta}. \quad (2)$$

Although modeling shows that relation (2) deviates from linear (e.g., Jameson 1992), the corresponding deviation usually is not very severe and many practical applications for simplicity use $\zeta = 1$.

Values of the coefficients α and γ are crucial for applications of correction schemes at attenuating radar frequencies (note that the range-profiling attenuation correction approach relates total attenuation and total propagation phase shift by means of α). Often these values are found through theoretical modeling assuming an oblate spheroidal raindrop shape, some mean drop aspect ratio (i.e., minor-to-major dimension ratio)–size relation, and parameters of drop canting. Modeling is performed either for theoretical drop size distributions (DSDs), such as gamma functions, with widely varying parameters (e.g., Gorgucci and Chandrasekar 2005), or for experimental distributions measured in situ by disdrometers (e.g., Matrosov 2010). The self-consistent correction techniques (e.g., Bringi et al. 2001; Park et al. 2005) for estimating α and γ from a theoretically determined range of their variability assume constancy of the a priori fixed exponent in the specific attenuation–reflectivity (A_h–Z_{eh}) power-law relations. This exponent is usually between 0.6 and 0.9 (e.g., Ryzhkov et al. 2014), and its relative variability is similar to the variability of the exponent in R–Z_{eh} relations, which are traditionally used for radar QPE.

The aforementioned approaches for deriving coefficients α and γ use various model assumptions about raindrop characteristics and/or relations between different radar variables. However, the actual mean drop shapes deviate from that of an oblate spheroid (e.g., Pruppacher and Klett 1978). Besides, drop oscillations, which are usually neglected, can perturb an assumed aspect ratio–size relation (e.g., Bringi et al. 2001). The exponent in the A_h–Z_{eh} relations also generally varies because of natural DSD variability.

Although these approaches are widely used for correcting attenuation and differential attenuation effects in X-band radar measurements, it is desirable to obtain direct estimates of the coefficients in relations (1) and (2) solely from measurements, thus avoiding model assumption uncertainties. Obtaining such estimates is the main objective of this study. Comparing experimentally found coefficients with those derived using different assumptions is helpful in assessing different existing approaches to correct for attenuation in radar measurements. The estimation approach used in this study takes advantage of simultaneous and collocated radar measurements at two frequencies for one of which attenuation effects in rain are negligible. Direct estimates from experimental data also allow for independent evaluation of the validity of the linear assumptions in attenuation and differential attenuation relations.

2. Observations

The dual-wavelength (λ_1 = 3.2 cm and λ_2 = 11 cm) observations of rainfall used in this study were collected by the Colorado State University–University of Chicago–Illinois State Water Survey (CSU–CHILL; http://www.chill.colostate.edu/w/CSU_CHILL) radar during a July–September 2013 project of observing rainfall in the High Park wildfire burn area located west of Fort Collins, Colorado. The X- and S-band channels of the radar share the same antenna system, which ensures collocation of beam centers, though the X-band beam is about 3 times narrower than the 1°-wide beam of the S-band channel. The S-band observations are performed in the alternate transmission mode, which implies fast switching between horizontal and vertical polarizations. At the X-band channel, which is a relatively new addition to the CSU–CHILL radar (Junyent et al. 2013), a simultaneous transmission–simultaneous receiving (STSR) measurement mode is used. Attenuation and differential attenuation in rain at S band are typically more than one order of magnitude smaller than at X band (e.g., Doviak and Zrnic 1993) and can usually be neglected compared to X-band attenuation effects in the collocated dual-frequency measurements.

Figure 1 shows an example of original plan position indicator (PPI) sector horizontal polarization reflectivity measurements during one of the High Park events observed by the CSU–CHILL radar on 18 July 2013. Reflectivity patterns at both wavelengths look similar, though generally smaller X-band Z_e values (compared to S band) are obvious at farther ranges. Note that the maximum range of CHILL X-band measurements is only 90 km, so no dual-wavelength data are available beyond this range.

An example of collocated center beam measurements for one of the azimuths is shown in Fig. 2. At shorter ranges, observed Z_{eh} and Z_{DR} at both frequencies have similar magnitudes, but the X-band values of these radar variables become progressively biased low compared to the S-band values as range and the observed X-band differential phase Φ_{DP} increase (Fig. 2a). The copolar correlation coefficient ρ_{hv} is rather high (>0.93) at both frequencies in the rain region for ranges closer than about 53 km (Fig. 2b), though S-band ρ_{hv} values are closer to 1 than X-band values measured in the STSR

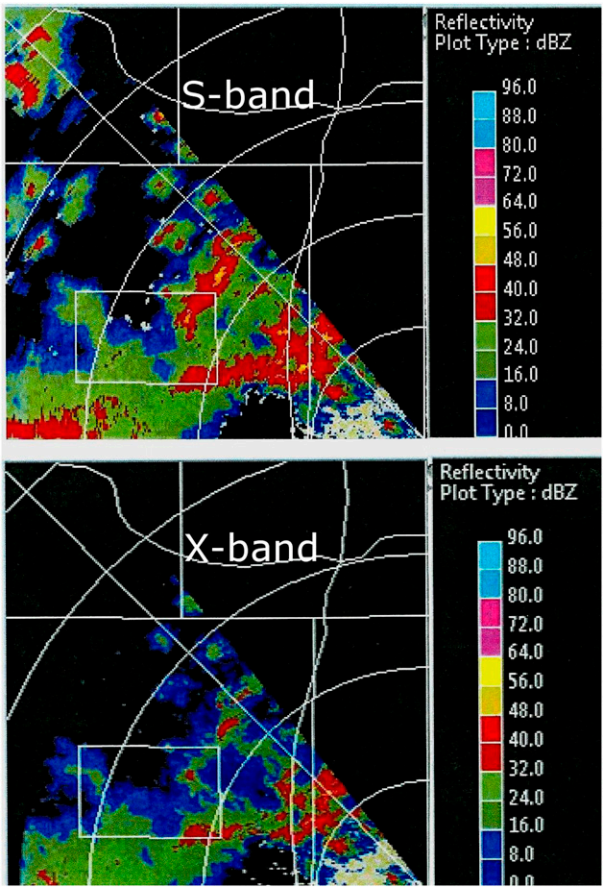

FIG. 1. An example of dual-wavelength [(top) S band, (bottom) X band] CHILL PPI reflectivity measurements (2202 UTC 18 Jul 2013, 1.7° elevation). Range rings are at 25-km increments. A white rectangle shows the High Park burn interest area.

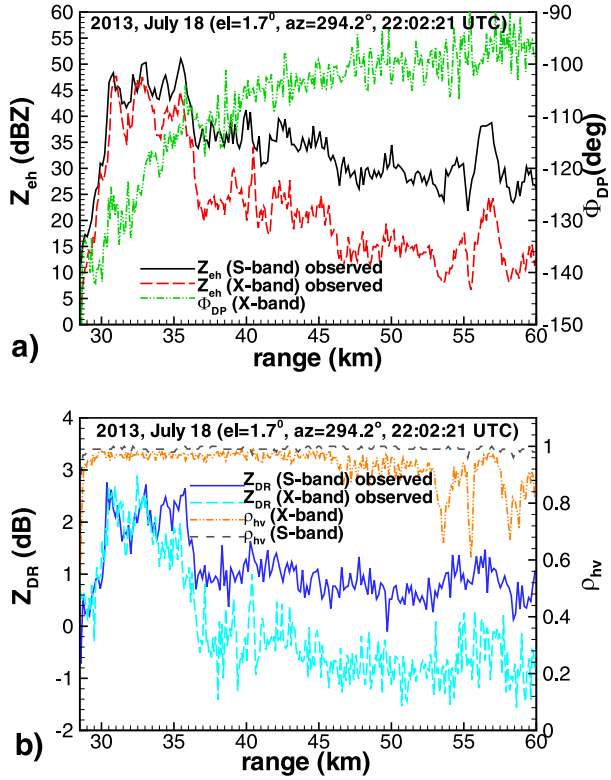

FIG. 2. An example of (a) S- and X-band reflectivity and (b) differential reflectivity measurements along the radar beam (elevation 1.7°, azimuth 294°) observed during the High Park project (2202 UTC 18 Jul 2013). X- and S-band copolar correlation coefficients ρ_{hv} and X-band differential phase $\Phi_{DP}(X)$ data are also shown.

mode. Beyond the range of 53 km, X-band ρ_{hv} drops mostly due to the low signal-to-noise ratio resulting from strong attenuation.

Although most features (e.g., Z_{eh} and Z_{DR} maxima/minima) in Fig. 2 look similar at both frequencies, their exact positions sometimes differ slightly, which might be a result of differing beamwidths and measurement noise. To reduce the influence of these factors in ensuing analyses, data averaging was performed. Such averaging can be performed in different ways. One way is to average the data in a regular X–Y coordinate grid. Figure 3 shows an example of gridded measurements when all data points with radar resolution volume centers within a given 1 km × 1 km cell in the larger area of interest were averaged. This was performed in linear scale (e.g., in $mm^6\,m^{-3}$ units for reflectivity data) when all data from gates within each grid box were averaged to obtain a gridded value. This gridding choice was convenient because the High Park radar measurements were further utilized to perform QPE retrievals for future use in testing hydrological models, which also required horizontal resolutions of QPE data of about 1 km.

While such Cartesian gridding reduces noisiness of the data, it is not expected to significantly bias estimations of the relations between attenuation (differential attenuation) and differential phase shift because these relations are quasi linear, as will be shown later. This gridding, however, results in averaging more points at close radar ranges than at far ranges. Averaging in the two-dimensional azimuth–range space avoids this issue (the corresponding gridding results are shown in Fig. 4) though data gridded in this space are not conveniently visualized as the Cartesian maps in Fig. 3. To assess the sensitivity of the results to the data averaging procedure, both types of gridding were performed here. Corresponding comparisons are shown in the next section.

Overall, six experimental events with significant attenuation of X-band radar signals in rain were observed during the High Park project. The significance of attenuation was judged by the magnitude of X-band

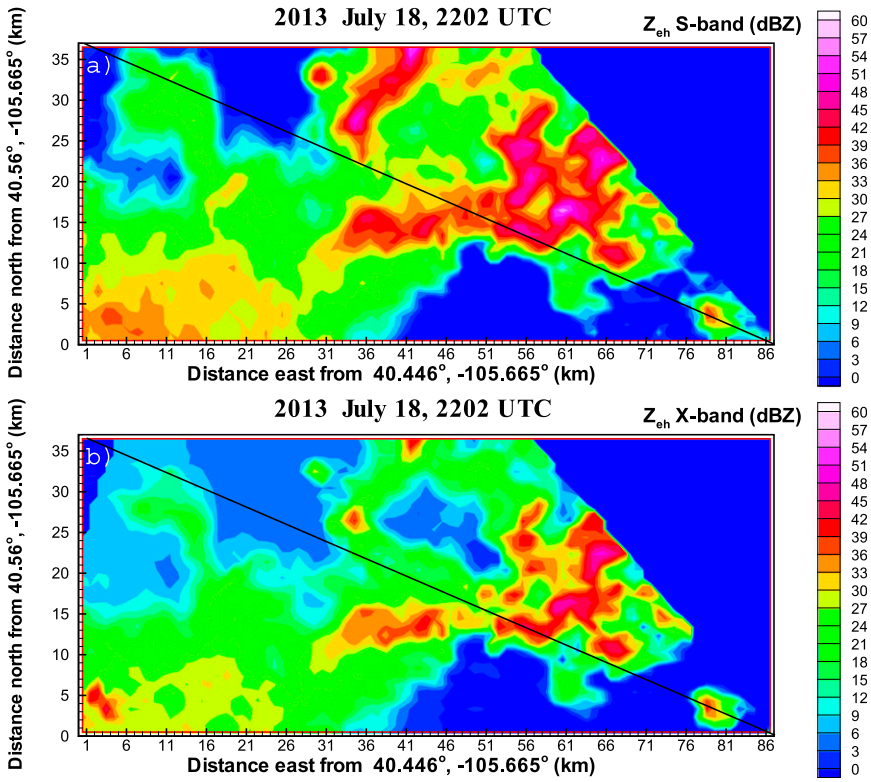

FIG. 3. Cartesian gridded measurements of (a) S-band and (b) X-band reflectivity (at an elevation of 1.7°) for a sector scan performed on 2202 UTC 18 Jul 2013. The location of the radar is at the bottom-right corner and the black line indicates the direction of beam shown in Fig. 2.

differential phase accumulation exceeding a threshold of 30°. A justification for this threshold value is given in the next section. Dual-wavelength reflectivity, differential reflectivity, and differential phase data gridding were performed for each of the events. Measurements from the lowest elevation beam tilt (~1.7°) that are essentially free of ground clutter were further used in this study. A typical interval between two consecutive sweeps at this elevation over the High Park area was about 2 min.

3. Estimation approaches and a case study of 18 July 2013

The rain event on 18 July 2013 lasted for about 5 h, that is, 164 gridded sector scans of the same type were constructed. Depending on the location, this event produced from approximately 15 to 50 mm of total rainfall in the High Park area and its vicinity. Figure 5 shows scatterplots of 1 km × 1 km gridded X-band differential phase $\Delta\Phi_{\mathrm{DP}}(\mathrm{X})$ and differences in both reflectivity and differential reflectivity (ΔZ and ΔZ_{DR}, respectively), which were defined as follows:

$$\Delta\Phi_{\mathrm{DP}}(\mathrm{X}) = \Phi_{\mathrm{DP}}(\mathrm{X}) - 136^\circ, \tag{3}$$

$$\Delta Z = Z_{eh}(\mathrm{S}) - Z_{eh}(\mathrm{X}), \quad \text{and} \tag{4}$$

$$\Delta Z_{\mathrm{DR}} = Z_{\mathrm{DR}}(\mathrm{S}) - Z_{\mathrm{DR}}(\mathrm{X}). \tag{5}$$

In (3) $\Phi_{\mathrm{DP}}(\mathrm{X})$ −136° is the gridded measured X-band differential phase and 136° is the estimated initial system phase due to the radar hardware. At each particular grid cell, $\Phi_{\mathrm{DP}}(\mathrm{X})$ consists of the propagation phase shift φ_{DP} and the backscatter phase shift δ_{hv} at the end of the propagation path to this grid cell:

$$\Phi_{\mathrm{DP}}(\mathrm{X}) = \varphi_{\mathrm{DP}}(\mathrm{X}) + \delta_{hv}(\mathrm{X}). \tag{6}$$

Since $\varphi_{\mathrm{DP}} = \int_0^{ro} K_{\mathrm{DP}}(r)\,dr$, where the integration is performed over the entire propagation path r_o, it is the $\varphi_{\mathrm{DP}}(\mathrm{X})$ contribution to the total phase $\Phi_{\mathrm{DP}}(\mathrm{X})$ that is related to the total path attenuation and differential attenuation.

The S-band values of $Z_{eh}(\mathrm{S})$ and $Z_{\mathrm{DR}}(\mathrm{S})$ were considered as estimates of nonattenuated reflectivity and differential reflectivity quantities at X band. Such an assumption for rain reflectivity is at least justified for

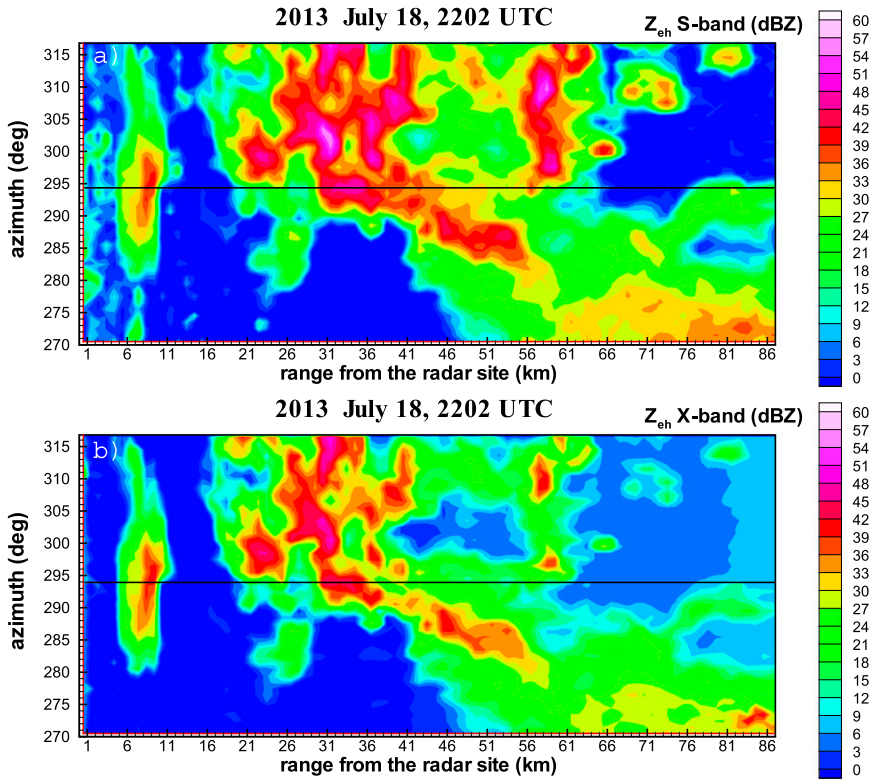

FIG. 4. Azimuth–range gridded measurements of (a) S-band and (b) X-band reflectivity (at an elevation of 1.7°) for a sector scan performed on 2202 UTC 18 Jul 2013. The location of the radar is at the bottom-left corner and the black line indicates the direction of beam shown in Fig. 2.

$Z_{eh}(\mathrm{S}) < 40\,\mathrm{dB}Z$. Below this threshold non-Rayleigh scattering effects at X band are rather small, so that typical differences between S- and X-band nonattenuated reflectivities are generally less than approximately 1 dB (Matrosov et al. 2006). Differences between S- and X-band nonattenuated differential reflectivities usually do not exceed 0.3 dB as long as mean mass-weighted drop diameters are smaller than approximately 2–2.5 mm (Matrosov et al. 2006). This range of drop sizes approximately typically corresponds to Z_{DR} values that are less than about 2 dB.

Additionally, Z_{DR} values less than 2 dB are expected to be associated with X-band backscatter differential phase δ_{hv}, which is less than approximately 3°. As a justification of this threshold, theoretical estimates of δ_{hv} obtained using DSDs collected in Colorado Front Range rainfall (Matrosov et al. 2006) similar to one observed during the High Park project are shown in Fig. 6. The δ_{hv} values results were calculated as described by Matrosov et al. (1999) but using experimental rather than theoretical DSDs. The 2-dB Z_{DR} threshold is also consistent with the results of Schneebeli and Berne (2012) and Trömel et al. (2013), which were based on different datasets.

Figure 5 shows the best-fit linear (solid lines) and power-law (dashed lines) fits for the relations $\Delta Z - \Delta\Phi_{\mathrm{DP}}(\mathrm{X})$ and $\Delta Z_{\mathrm{DR}} - \Delta\Phi_{\mathrm{DP}}(\mathrm{X})$, respectively. To minimize the nonattenuated reflectivity differences at X and S bands and also to minimize the influence of backscatter phase shift, these relations were drawn for the subset of data points, which satisfy the threshold conditions $Z_{eh}(\mathrm{S}) < 40\,\mathrm{dB}Z$, $Z_{\mathrm{DR}}(\mathrm{S}) < 2\,\mathrm{dB}$, $\Delta\Phi_{\mathrm{DP}}(\mathrm{X}) > 30°$, $\rho_{hv}(\mathrm{X}) > 0.9$ (even though all rain data points are shown in Fig. 5). The condition $\rho_{hv}(\mathrm{X}) > 0.9$ ensures that data points with a low signal-to-noise ratio (SNR), resulting in unreliable reflectivity estimates (e.g., X-band reflectivity near the end of the radar beam in Fig. 2), are not used. Because attenuation in melting hydrometeors is quite different from that in rain (e.g., Matrosov 2008), excluded from the analysis were also data at longer ranges, where upper edges of the radar beams were expected to be within or above the melting layer.

The thresholding condition $\Delta\Phi_{\mathrm{DP}}(\mathrm{X}) > 30°$ was used to minimize possible effects of δ_{hv} and the noise in differential phase measurements, which is typically around 1.5°– 2° (Matrosov et al. 2002). The hydrometeor identification (HID) analysis was performed for the data used in this study. The HID membership functions were adopted from Dolan and Rutledge (2009). The HID analysis confirmed that the precipitation data points in

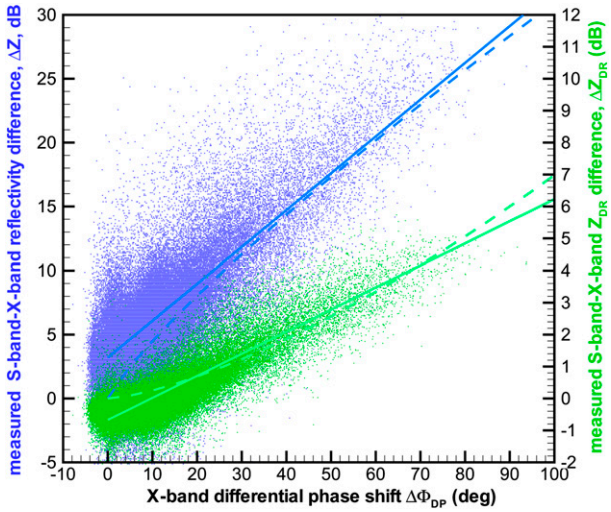

FIG. 5. Scatterplots of measured S band–X band of reflectivity (blue) and differential reflectivity (green) differences vs measured X-band differential phase for the event of 18 Jul 2013 data gridded in 1 km × 1 km cells. Solid (dashed) lines show best linear (power law) fit relations for conditions $Z_e(\mathrm{S}) < 40\,\mathrm{dB}Z$, $Z_{\mathrm{DR}}(\mathrm{S}) < 2\,\mathrm{dB}$, $\Delta\Phi_{\mathrm{DP}}(\mathrm{X}) > 30°$, and $\rho_{hv}(\mathrm{X}) > 0.9$.

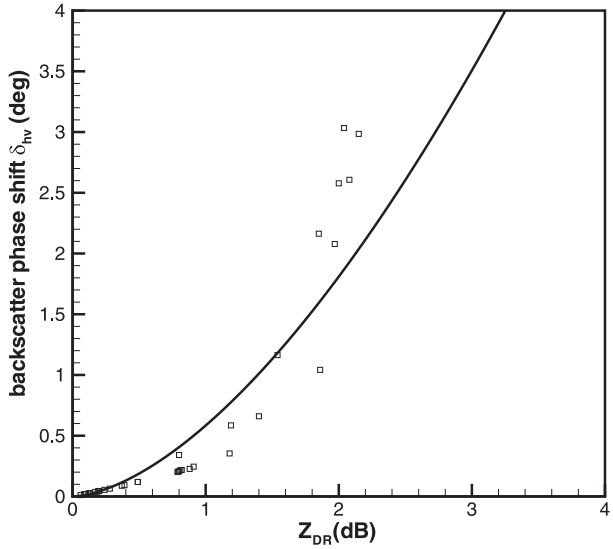

FIG. 6. Estimates of the backscatter phase shift at X band as a function of differential reflectivity. Symbols show modeling results and the solid line corresponds to the best power-law fit.

the Fig. 5 scatterplot overwhelmingly (>96%) correspond to rain. Although these authors provide membership functions for both S- and X-band measurements, only the "nonattenuated" S-band data were used in this study for the HID purpose.

As seen in Fig. 5 the differences in the best linear and power-law fits are rather small compared to overall data scatter. This scatter relative to the best-fit approximation data expressed in the standard deviation amounts to approximately 3.1 and 0.6 dB for ΔZ and ΔZ_{DR}, respectively. Given the high level of agreement between the linear and power-law approximations, the linear fits were used hereafter. Based on the linear assumption and neglecting δ_{hv}, as it is expected to be at least an order of magnitude smaller than the propagation phase shift for $\Delta\Phi_{\mathrm{DP}}(\mathrm{X}) > 30°$, the following expressions for reflectivity and differential reflectivity differences can be written as

$$\Delta Z = \alpha\Delta\Phi_{\mathrm{DP}}(\mathrm{X}) + \Delta Z_0, \tag{7}$$

$$\Delta Z_{\mathrm{DR}} = \gamma\Delta\Phi_{\mathrm{DP}}(\mathrm{X}) + \Delta Z_{\mathrm{DR0}}. \tag{8}$$

The quantities ΔZ_0 and ΔZ_{DR0} can be regarded as offsets due to calibration and/or differing radome influences. The values of the coefficients in the linear relations between specific attenuation (differential attenuation) and specific differential phase shift for the 18 July 2013 rain event (Fig. 5) are $\alpha \approx 0.288\,\mathrm{dB\,deg^{-1}}$ and $\gamma \approx 0.06\,\mathrm{dB\,deg^{-1}}$, respectively.

Figure 7 shows the scatterplot for 18 July 2013 data when the azimuth–range averaging procedure instead of the 1 km × 1 km cell gridding scheme was performed. To implement this procedure, data were gridded in 1° azimuth and 1-km range intervals. Since 1° azimuth averaging approximately corresponds to the S-band beamwidth, three X-band beams were typically averaged to match one beam of S-band data. Azimuthal gridding also allowed for convenient removal of data points with propagation paths where rain attenuation estimates could have been contaminated by the presence of graupel. The data points were removed from the analysis if the range to

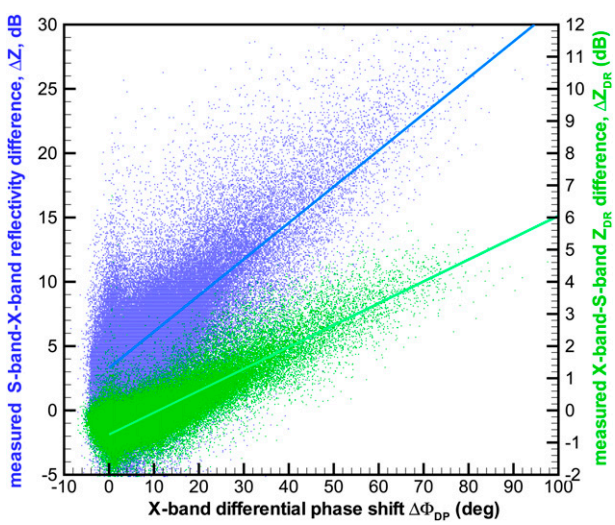

FIG. 7. As in Fig. 5, but for the azimuth–range averaged data.

TABLE 1. Estimated coefficients in the linearized $A_h = \alpha K_{DP}$ and $A_{DP} = \gamma K_{DP}$ relations for different events.

Event date	12 Jul 2013	18 Jul 2013	25 Jul 2013	28 Jul 2013	3 Aug 2013	12 Sep 2013
Event duration (h)	2.5	3.0	6.0	1.7	3.7	9.0
α (dB deg^{-1})	0.252	0.281	0.202	0.270	0.308	0.240
γ (dB deg^{-1})	0.063	0.058	0.056	0.065	0.057	0.052

those points contained precipitation identified by the HID algorithm as graupel, and the path-integrated reflectivity of suspected graupel intervals was at least 10% of the total path-integrated reflectivity. The best-fit linear relation coefficients in (7) and (8) for the scatterplot in Fig. 7 are $\alpha \approx 0.281$ dB deg^{-1}, and $\gamma \approx 0.058$ dB deg^{-1}, respectively, which is not much different from the values for those coefficients obtained with the 1 km × 1 km gridding scheme. The data scatter in Figs. 5 and 7 is also very similar. These results indicate that the values of the retrieved coefficients were not very sensitive to the gridding technique.

4. Statistics of experimental attenuation phase relations

All experimental events observed by the CHILL radar during the High Park project, which resulted in significant X-band signal attenuation effects, were processed in a manner described for the 18 July 2013 case study. The estimated values of the coefficients α and γ for all events assuming linear relations between specific attenuation (differential attenuation) and specific differential phase shift are listed in Table 1 and the corresponding linear fits are shown in Fig. 8, which is a graphical representation of these table data. Even though this figure shows A_h–K_{DP} and A_{DP}–K_{DP} relations, the derivation of the coefficients in this relation did not involve K_{DP} calculations, which generally contain additional uncertainties.

The coefficient values described above were derived using the ρ_{hv}, reflectivity, Z_{DR}, and Φ_{DP} threshold conditions mentioned in section 3. The use of all data points having high ρ_{hv} [without thresholding on Z_{eh}(S), Z_{DR}(S), and $\Delta\Phi_{DP}$(X)] can result in about 10% variability of the coefficients from values shown in Table 1. A similar variability in the coefficients is present when the spatial scale of measurement averaging varied by ±50%.

While there are differences between the attenuation and differential attenuation corrections obtained with coefficients derived for different experimental events, these differences, at least for moderate values of accumulated differential phase (<60°), are comparable with the stated above-mentioned typical magnitudes of the individual point data scatter as shown in Figs. 5 and 7.

The values of the coefficient α for A_h–K_{DP} relations derived in this study solely from measurements agree relatively well with results from theoretical modeling (e.g., Matrosov 2010), which yielded values between about 0.23 and 0.28 dB deg^{-1} obtained using different drop mean axis ratio models and DSD datasets. These results also agree in a mean sense with estimates from the self-consistency technique used for X-band radar measurements by Park et al. (2005), who report a mean value of 0.254 dB deg^{-1} for α. Found in this study are values of the coefficient α that are generally somewhat smaller than the theoretical value of 0.313 dB deg^{-1} from Snyder et al. (2010).

Values of the coefficient γ (see Table 1) estimated here directly from measurements are somewhat higher than the theoretical results for this coefficient (~0.04–0.05 dB deg^{-1}) from Matrosov (2010) and Snyder et al. (2010). It cannot be ruled out, however, that part of the differences between the theoretical results and those found directly from dual-wavelength data may be due to cross-polarization coupling effects (e.g., Hubbert et al. 2010), which could affect X-band Z_{DR} measurements, which are conducted in the STSR measurement mode.

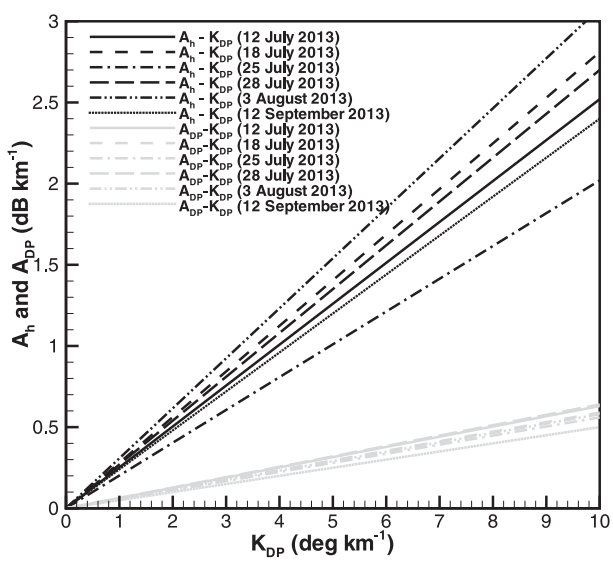

FIG. 8. X-band (λ = 3.2 cm) attenuation (black lines) and differential attenuation (gray lines) corrections obtained experimentally using data from different events assuming linearity of the correction coefficients relative to specific differential phase shift.

For most of the July–August events, precipitation was predominately convective in nature, although relatively short periods of moderate rainfall with a reflectivity bright band, which is characteristic of stratiform-type rain, were present during some of these events as revealed by occasional range–height indicator scans (not shown). The brightband features occurred frequently during the event of 12 September 2013. No special attempt of separating the results based on the precipitation types was performed because of uncertainties in discriminating local convective–stratiform features on short time scales. All the analyzed events were relatively warm with similar ground air temperatures of around 15°C. Thus, no temperature dependencies of the coefficients α and γ were analyzed.

5. Conclusions

The use of radars operating at attenuating frequencies (e.g., X band) for meteorological applications including QPE is now common. Such radars are utilized for research purposes and for filling gaps in operational radar coverage. Networks of inexpensive X-band radars are also used for high-resolution precipitation mapping (e.g., McLaughlin et al. 2009). X-band radar measurements, however, require corrections of reflectivity and differential reflectivity data for attenuation and differential attenuation in rain. The most common approach for such corrections is based on relations between attenuation (and differential attenuation) and differential phase between horizontally and vertically polarized radar signals. Usually such relations are assumed to be linear and their coefficients are found through theoretical modeling for idealized drop shapes and a set of assumptions about drop mean aspect ratios and DSDs and/or through range-profiling schemes that use assumptions about relations between specific attenuation and reflectivity.

The experimentally based approach to estimate coefficients in such relations uses S- and X-band dual-wavelength polarimetric radar measurements of rainfall during a field project in northern Colorado. The main advantage of the approach is that it is essentially free of modeling assumptions about drop shapes, their oscillation modes, size distributions, and relations between attenuation characteristics and reflectivity. The attenuation effects at S band are neglected compared to those at X band, so lower-frequency measurements provide "nonattenuated" references for higher-frequency data. To minimize the effects of non-Rayleigh scattering and backscatter differential phase shift at X band, the dataset used for deriving coefficients was limited to the values of nonattenuated reflectivities below 40 dBZ and differential reflectivities below 2 dB. The measurements with higher X-band differential phase accumulations (>30°) were used for deriving coefficients in the sought relations to further reduce influences of backscatter phase shift.

As a result of the application of this approach to a number of events, it is shown that the linear approximations for the horizontal polarization specific attenuation A_h and specific differential attenuation A_{DP} as functions of specific differential phase K_{DP} are generally adequate given data scatter/noise, which, in terms of the standard deviation, is on the order of approximately 3.1 and 0.6 dB for the S–X-band reflectivity and differential reflectivity differences (for a given value of the differential phase), respectively. The values of the coefficient α in the attenuation–differential phase relation and the coefficient γ in differential attenuation–differential phase relations were found to vary in a range approximately between 0.20 and 0.31 dB deg^{-1} for α and about 0.051 and 0.065 dB deg^{-1} for γ. This range of α values found solely from measurements is in general agreement with results found in other studies using different assumptions, although the estimated values of γ derived in this study are somewhat higher than those derived with modeling assumptions.

Acknowledgments. This study was funded in part by the NOAA Hydrometeorology Testbed (HMT) project. The data collection was performed by the CSU–CHILL radar.

REFERENCES

Anagnostou, E. N., M. N. Anagnostou, W. Krajewski, A. Kruger, and B. J. Mirovsky, 2004: High-resolution rainfall estimation from X-band polarimetric radar measurements. *J. Hydrometeor.,* **5,** 110–128, doi:10.1175/1525-7541(2004)005<0110:HREFXP>2.0.CO;2.

Bringi, V. N., and V. Chandrasekar, 2001: *Polarimetric Doppler Weather Radar*. Cambridge University Press, 636 pp.

——, T. D. Keenan, and V. Chandrasekar, 2001: Correcting C-band radar reflectivity and differential reflectivity data for rain attenuation: A self-consistent method with constraints. *IEEE Trans. Geosci. Remote Sens.,* **39,** 1906–1915, doi:10.1109/36.951081.

Dolan, B., and S. A. Rutledge, 2009: A theory-based hydrometeor identification algorithm for X-band polarimetric radars. *J. Atmos. Oceanic Technol.,* **26,** 2071–2088, doi:10.1175/2009JTECHA1208.1.

Doviak, R. J., and D. S. Zrnic, 1993: *Doppler Radar and Weather Observations*. Academic Press, 562 pp.

Gorgucci, E., and V. Chandrasekar, 2005: Evaluation of attenuation correction methodology for dual-polarization radars: Application to X-band systems. *J. Atmos. Oceanic Technol.,* **22,** 1195–1206, doi:10.1175/JTECH1763.1.

Hubbert, J. C., S. M. Ellis, M. Dixon, and G. Meymaris, 2010: Modeling, error analysis, and evaluation of dual-polarization

variables obtained from simultaneous horizontal and vertical transmit radar. Part I: Modeling and antenna errors. *J. Atmos. Oceanic Technol.,* **27,** 1583–1598, doi:10.1175/2010JTECHA1336.1.

Jameson, A. R., 1992: The effect of temperature on attenuation-correction schemes in rain using polarization propagation differential phase shift. *J. Appl. Meteor.,* **31,** 1106–1118, doi:10.1175/1520-0450(1992)031<1106:TEOTOA>2.0.CO;2.

Junyent, F., V. Chandrasekar, P. Kennedy, S. Rutledge, V. Bringi, J. George, and D. Brunkow, 2013: Salient features of the CSU-CHILL radar X-band channel upgrade. *36th Conf. on Radar Meteorology,* Breckenridge, CO, Amer. Meteor. Soc., 2B.6. [Available online at https://ams.confex.com/ams/36Radar/webprogram/Paper229162.html.]

Matrosov, S. Y., 2008: Assessment of radar signal attenuation caused by the melting hydrometeor layer. *IEEE Trans. Geosci. Remote Sens.,* **46,** 1039–1047, doi:10.1109/TGRS.2008.915757.

——, 2010: Evaluating polarimetric X-band radar rainfall estimators during HMT. *J. Atmos. Oceanic Technol.,* **27,** 122–134, doi:10.1175/2009JTECHA1318.1.

——, R. A. Kropfli, R. F. Reinking, and B. E. Martner, 1999: Prospects for measuring rainfall using propagation differential phase in X- and K_a- radar bands. *J. Appl. Meteor.,* **38,** 766–776, doi:10.1175/1520-0450(1999)038<0766:PFMRUP>2.0.CO;2.

——, K. A. Clark, B. E. Martner, and A. Tokay, 2002: X-band polarimetric radar measurements of rainfall. *J. Appl. Meteor.,* **41,** 941–952, doi:10.1175/1520-0450(2002)041<0941:XBPRMO>2.0.CO;2.

——, R. Cifelli, P. C. Kennedy, S. W. Nesbitt, S. A. Rutledge, V. N. Bringi, and B. E. Martner, 2006: A comparative study of rainfall retrievals based on specific differential phase shifts at X- and S-band radar frequencies. *J. Atmos. Oceanic Technol.,* **23,** 952–963, doi:10.1175/JTECH1887.1.

McLaughlin, D., and Coauthors, 2009: Short-wavelength technology and the potential for distributed networks of small radar systems. *Bull. Amer. Meteor. Soc.,* **90,** 1797–1817, doi:10.1175/2009BAMS2507.1.

Park, S.-G., M. Maki, K. Iwanami, V. N. Bringi, and V. Chandrasekar, 2005: Correction of radar reflectivity and differential reflectivity for rain attenuation at X band. Part II: Evaluation and application. *J. Atmos. Oceanic Technol.,* **22,** 1633–1655, doi:10.1175/JTECH1804.1.

Pruppacher, H. R., and J. D. Klett, 1978: *Microphysics of Clouds and Precipitation.* D. Reidel, 714 pp.

Ryzhkov, A. V., M. Diederich, P. Zhang, and C. Simmer, 2014: Potential utilization of specific attenuation for rainfall estimation, mitigation of partial beam blockage, and radar networking. *J. Atmos. Oceanic Technol.,* **31,** 599–619, doi:10.1175/JTECH-D-13-00038.1.

Schneebeli, M., and A. Berne, 2012: An extended Kalman filter framework for polarimetric X-band weather radar data processing. *J. Atmos. Oceanic Technol.,* **29,** 711–730, doi:10.1175/JTECH-D-10-05053.1.

Snyder, J. C., H. B. Bluestein, G. Zhang, and S. J. Frasier, 2010: Attenuation correction and hydrometeor classification of high-resolution, X-band, dual-polarized mobile radar measurements in severe convective storms. *J. Atmos. Oceanic Technol.,* **27,** 1979–2001, doi:10.1175/2010JTECHA1356.1.

Testud, J., E. Le Bouar, E. Obligis, and M. Ali-Mehenni, 2000: The rain profiling algorithm applied to polarimetric weather radar. *J. Atmos. Oceanic Technol.,* **17,** 332–356, doi:10.1175/1520-0426(2000)017<0332:TRPAAT>2.0.CO;2.

Trömel, S., M. R. Kumjian, A. V. Ryzhkov, C. Simmer, and M. Diederich, 2013: Backscatter differential phase—Estimation and variability. *J. Appl. Meteor. Climatol.,* **52,** 2529–2548, doi:10.1175/JAMC-D-13-0124.1.